Volume 61
Number 46
11 June 2025
Pages 8283–8448

ChemComm

Chemical Communications

rsc.li/chemcomm

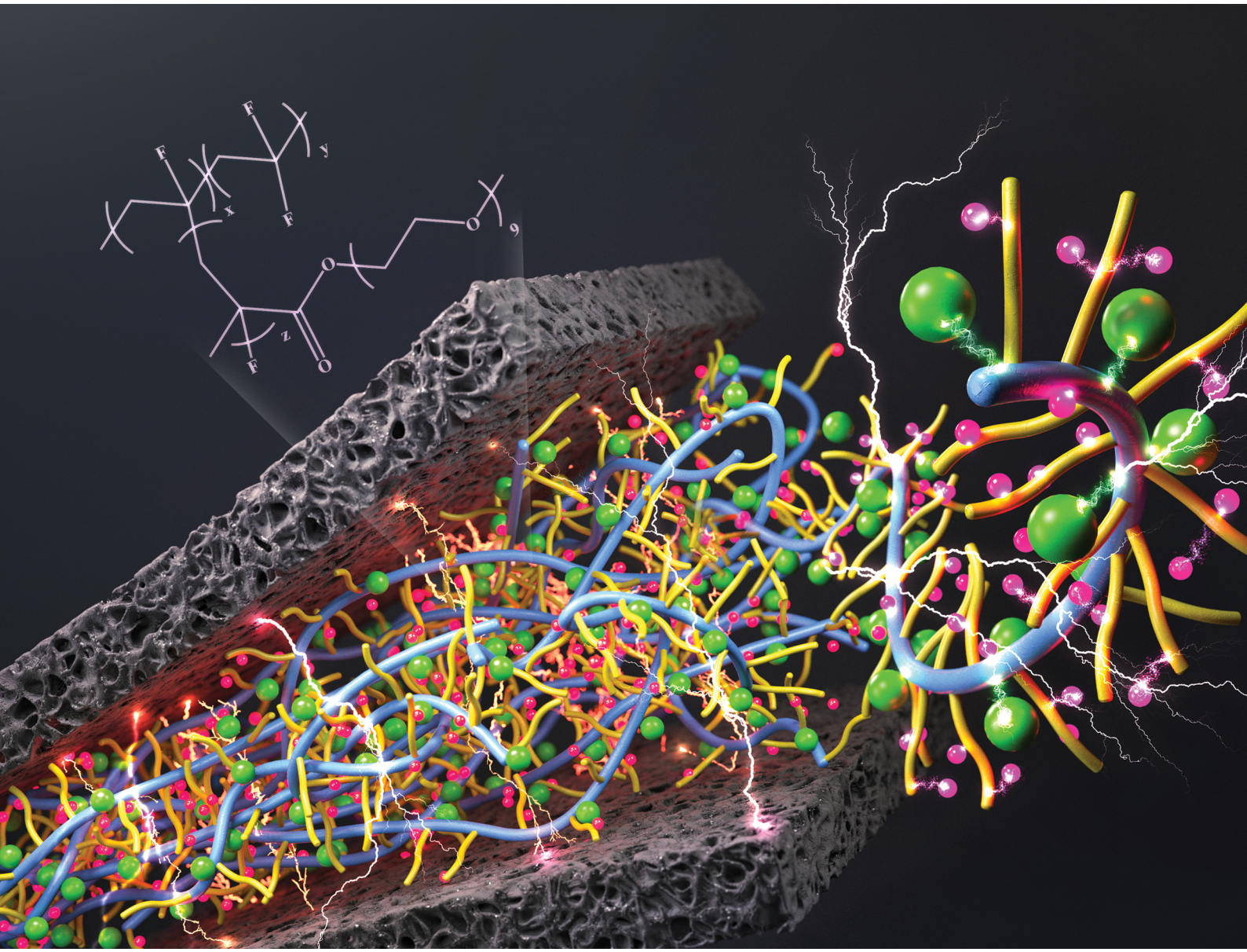

ISSN 1359-7345

ROYAL SOCIETY OF CHEMISTRY

COMMUNICATION

Jung Tae Park *et al.*

An amphiphilic PVDF-*g*-POEM double comb copolymer-based solid-state electrolyte for EDLC applications: electrochemical and electrical property studies

ChemComm

COMMUNICATION

View Article Online
View Journal | View Issue

Cite this: *Chem. Commun.*, 2025, 61, 8339

Received 15th March 2025,
Accepted 6th May 2025

DOI: 10.1039/d5cc01490e

rsc.li/chemcomm

An amphiphilic PVDF-*g*-POEM double comb copolymer-based solid-state electrolyte for EDLC applications: electrochemical and electrical property studies†

Uoon Chul Baek,[a] Da Hye Sim[b] and Jung Tae Park *[a]

A modified polyvinylidene fluoride (PVDF)-based electrolyte, amphiphilic polyvinylidene fluoride-*graft*-poly(ethylene glycol)methyl ether methacrylate (PVDF-*g*-POEM), double comb copolymer is synthesized for use as a solid-state electrolyte within an electric double layer capacitor (EDLC). The double comb copolymer is synthesized *via* atom transfer radical polymerization (ATRP). The solid-state electrolyte prepared using the amphiphilic PVDF-*g*-POEM double comb copolymer shows increased ionic conductivities, compared to that of the hydrophobic PVDF-based electrolyte. Incorporating hydrophilic POEM chains into semi-crystalline hydrophobic PVDF results in nanophase separation and decreased polymer crystallinity, yielding facile ion transport pathways and enhancing the ionic conductivity. The electrochemical and electrical characteristics of the prepared EDLC cells are investigated using cyclic voltammetry, galvanostatic charge–discharge cycling, and impedance spectroscopy. The specific capacitance of 38.07 F g^{-1} (0.5 A g^{-1}) was achieved with an energy density of 25.59 W h kg^{-1} at a power density of 0.275 kW kg^{-1}. After 8000 cycles (1 A g^{-1}), the cells show a capacitive retention of 95.6%, with an 85% coulombic efficiency.

Electric double layer (EDL)-type supercapacitors are candidates to replace traditional energy storage systems. Owing to the lack of faradaic redox chemistry within the EDL capacitors (EDLCs), a variety of merits, such as low preparation cost, high power delivery, and high cycling stability, have attracted attention for decades.[1–4] Although the performance gap between the supercapacitor and battery has been successfully filled in recent years, the development of supercapacitors with higher energy densities, using sustainable and non-hazardous methods, remains necessary.[5–7]

Classically, electrolytes within energy devices are liquid-based, with several related issues, such as leakage and flammability.[8,9] Within supercapacitors, the most common electrolytes are water-based, as these are the simplest to prepare, with high ionic conductivities. Yet, aqueous electrolytes exhibit thermodynamically limited voltage windows of 1.23 V, due to electrolysis of the water during long-term device operation.[10] In contrast, organic electrolytes and ionic liquids exhibit superior promise, with broader voltage windows but volatility and flammability problems.[11,12] One approach to address these issues is to prepare cells incorporating solid-state or gel-type polymer electrolytes, with the type being dependent on the characteristics of the polymer matrix. These lightweight polymer electrolytes provide several further advantages over liquid electrolytes, such as facile processability and excellent safety, with leakage or shortage of the devices prevented.[13] Conversely, the main issues of the polymer electrolytes are low conductivities, insufficient mechanical properties, and price competitiveness compared to those of liquid systems, which hinder their practical applications.[14]

To obtain polymer based solid-state electrolytes with excellent properties, the polymer should meet several criteria, including (i) fast segmental motion of the polymer chain, (ii) bearing special groups inducing salt dissolution, (iii) low glass transition temperature, (iv) high molecular weight, (v) wide electrochemical stability window, and (vi) high thermal stability.[14,15] To tune the polymer properties, polymeric frameworks are modified using various methods: copolymerization, blending, and adding or incorporating composite materials.[16–18] Recent studies have demonstrated promising results using lithium- and sodium-ion conducting polymer electrolytes in EDLC configurations. For instance, a PAN–LiBOB-based electrolyte showed improved conductivity and capacitive performance when applied to an EDLC device,[19] while a green sodium-ion conducting chitosan–PVA-based nanocomposite demonstrated a wide electrochemical window and high energy density.[20]

In this study, hydrophilic PEO-based polymer, poly(ethylene glycol)methyl ether methacrylate (POEM) was grafted onto the hydrophobic PVDF main chain to form an amphiphilic double comb copolymer, PVDF-*graft*-POEM (PVDF-*g*-POEM), *via* ATRP.

[a] *Department of Integrated Display Engineering, Yonsei University, 50 Yonsei-ro, Seodaemun-gu, Seoul 03722, Republic of Korea. E-mail: jtpark25@yonsei.ac.kr*
[b] *Department of Chemical and Biomolecular Engineering, Yonsei University, 50 Yonsei-ro, Seodaemun-gu, Seoul 03722, Republic of Korea*

† Electronic supplementary information (ESI) available. See DOI: https://doi.org/10.1039/d5cc01490e

This copolymer was designed for use as a polymer electrolyte, which serves as a solid-state electrolyte for EDLC applications. Grafting of hydrophilic POEM chains to hydrophobic PVDF macroinitiator chains may induce nanophase separation of the polymers, which should yield superior ionic conduction pathways for the incorporated lithium bis(trifluoromethanesulfonimide) (LiTFSI), producing improved electrolyte performance.[19–21] Such amphiphilic architectures are known to facilitate ionic conductivity through phase-separated ion channels while maintaining mechanical properties.[22,23] Furthermore, the degree of crystallinity of the semi-crystalline PVDF may be lowered by the grafting of the POEM chain, yielding higher polymer segmental motion. The structures and morphologies of the double comb copolymers, including its applications to solid-state electrolytes in EDLC, and its electrochemical and electrical properties, were studied.

Scheme 1(a) and (b) show the synthesis of PVDF-*g*-POEM *via* ATRP and its application to EDLC. Initiated by the fluorine atoms, hydrophilic POEM side chains are grafted onto the hydrophobic PVDF backbone by ATRP. The amphiphilic PVDF-*g*-POEM double comb copolymer contains the hydrophobic semi-crystalline regions of the PVDF main chains that self-assemble by nanophase separation from the hydrophilic domains of the POEM brush layers. This leads to effective control of the formation of Li and TFSI ion transfer pathways and lowers the crystallinity of the PVDF polymer, which is favourable for solid-state electrolyte performance.[24]

The copolymerization of POEM side chains with the PVDF backbone *via* ATRP is confirmed using ^{1}H-NMR spectroscopy, as shown in Fig. 1(a). The ^{1}H-NMR spectrum of the amphiphilic PVDF-*g*-POEM double comb copolymer is displayed in the inset, where the mole and weight fractions of POEM were determined to be 1% and 5%, respectively, after a reaction time of 24 hours, using eqn (S1) and (S2) (ESI†). Fig. 1(b) shows the thermal characteristics of the PVDF backbone and amphiphilic PVDF-*g*-POEM double comb copolymer, which were investigated using

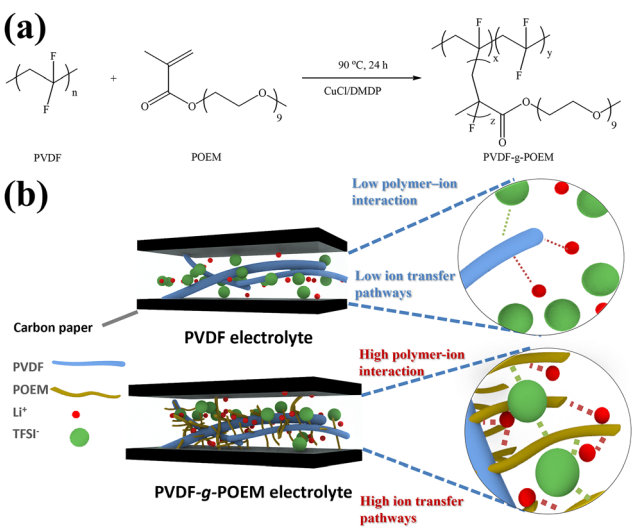

Scheme 1 (a) Illustration of the synthesis of the amphiphilic PVDF-*g*-POEM double comb copolymers *via* atom transfer radical polymerization and (b) EDLC cells with solid-state electrolytes.

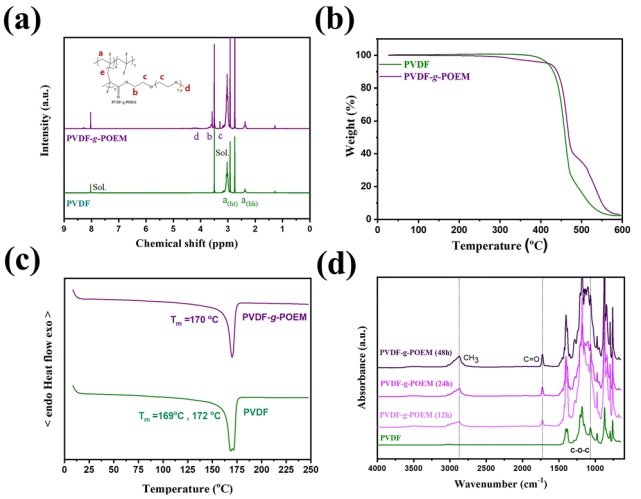

Fig. 1 (a) ^{1}H-NMR spectra of the hydrophobic PVDF and amphiphilic PVDF-g-POEM double comb copolymer and (b) TGA curves of the polymer under air conditions. (c) 2nd cycle of the DSC curves of the hydrophobic PVDF and amphiphilic PVDF-*g*-POEM double comb copolymer. And (d) FT-IR spectra of the hydrophobic PVDF and amphiphilic PVDF-*g*-POEM double comb copolymer with different reaction periods.

TGA. The TGA thermograms are plotted as a function of temperature with a heating rate of 5 °C min^{-1} from 25 °C to 600 °C under an air atmosphere. The obtained double comb copolymer demonstrates the thermal-decomposition characteristics of both PVDF and POEM. Pure PVDF commences decomposition at >420 °C, whereas the double comb copolymer decomposes in two steps, with the first mass loss at >250 °C. At the onset of decomposition, the observed temperature is characteristic of POEM, with the calculated mass of the POEM chains from ^{1}H-NMR spectroscopy (5 wt%) consistent with this mass loss. Furthermore, at >440 °C, the sample exhibits PVDF characteristics. The structural thermal properties of the polymers were analysed using DSC, with the thermograms shown in Fig. 1(c). The melting point, enthalpy of fusion and crystallinity data are listed in Table S1 (ESI†). Compared to PVDF, which exhibits an enthalpy of fusion, ΔH_f, of 51.02 J g^{-1}, the double comb copolymer displays a significantly lower ΔH_f of 26.26 J g^{-1} due to a decrease in crystallinity (χ_c) of 48.7% for PVDF and 26.3% for the double comb copolymer.[25] Note that the reduced crystallinity contributes to enhanced performance of the solid-state electrolytes in electrochemical devices.[26,27] Fig. 1(d) shows the FT-IR spectra of hydrophilic PVDF and the amphiphilic PVDF-*g*-POEM double comb copolymer synthesized *via* ATRP. The FT-IR spectra of purified PVDF-*g*-POEM prepared using different reaction times, along with those of the PVDF and POEM are shown. The appearance of the peaks at 2872, 1723, and 1105 cm^{-1} corresponding to the skeletal breathing of CH_3 (methyl) and C═O (carbonyl) and C–O–C ester stretches, respectively, indicates that POEM branches are grafted onto the PVDF chains. Furthermore, the intensities of these peaks increase as the polymerization time increases from 12 to 48 h, demonstrating the controllable nature of the ATRP.[24] Conversely, the absence of a peak at 1640 cm^{-1}, representing C═C stretching, suggests that

the unreacted POEM macromonomer is successfully removed during washing. These FT-IR spectra are clear evidence of the sequential synthesis of the graft copolymer *via* ATRP.[28]

The ionic conductivities of the samples containing different contents of LiTFSI ions, calculated using the bulk resistance (R_s) obtained from the Nyquist plots shown in Fig. 2(a), are presented. The inset illustrates the simplified RC circuit for polymer electrolytes, which includes a series resistance, or bulk resistance in this case (R_s) and a parallel combination of a constant phase element (C_{dl}) and an interfacial resistance (R_i). While R_s remains relatively constant across the samples, variations in the overall impedance suggest changes in R_i influenced by the LiTFSI content. The thermal behaviour of the electrolytes was investigated, as shown by the Arrhenius plot in Fig. 2(b), with the behaviours of the polymer following the well-known Arrhenius relationship from the equation in the ESI† (eqn (S10)). The activation energy of ion conduction within the polymer electrolyte is calculated using this equation, exhibiting the common trend of increasing conductivity with increasing temperature. The activation energy of the amphiphilic PVDF-*g*-POEM double comb copolymer based solid-state electrolyte with the optimal concentration of 15 wt% LiTFSI (0.207 eV) is lower than that of bare PVDF (0.387 eV). Thus, facile ionic transport within the amphiphilic PVDF-*g*-POEM double comb copolymer compared to that within the bare PVDF matrix is expected due to the synergetic effect of the increase in the amorphous nature of the amphiphilic copolymer, and the nanophase-separated structure of the polymer matrix. The ionic conductivities of the samples containing different contents of LiTFSI ions are shown in Fig. 2(c) and listed in Table S2 (ESI†). A critical factor affecting the conductivity of the polymer is the salt concentration. The maximum conductivity is observed at 15 wt% LiTFSI content (9.23×10^{-4} S cm^{-1}). Higher LiTFSI contents lead to deterioration of ionic conductivity due to a combination of increased viscosity, which limits ion mobility despite the greater number of charge carriers, and the formation of Li^+ ion pairs within the solid-state electrolyte membrane, which reduces the number of free charge carriers.[29,30]

To investigate the effectiveness of the amphiphilic PVDF-*g*-POEM double comb copolymer as a solid-state electrolyte, flexible EDLCs were prepared using conventional carbon-based electrodes containing a mixed carbon slurry (activated carbon, carbon black, and a PVDF binder) on carbon paper substrates. It is noteworthy that trace amounts of residual solvents such as DMF might persist even after extensive drying due to their high boiling points, which can facilitate ionic conduction by maintaining the electrolyte in a gel-like state.[31] Nonetheless, since both the control and the experimental electrolytes were identically processed, such solvent-related effects are expected to equally influence both systems. However, the cyclic voltammogram shown in Fig. 3(a) reveals deterioration of the residual DMF solvent-plasticizer within the polymer gel at voltages >2.2 V, thus limiting the voltage window to 0–2.2 V for the symmetric capacitor. The cyclic voltammograms of the EDLC cells are plotted at different scan rates within the voltage window 0.0–2.2 V in Fig. 3(b). The specific capacitances (F g^{-1}) of the devices are calculated based on CV. The cell based on the amphiphilic PVDF-*g*-POEM double comb copolymer based solid-state electrolyte exhibits the thicker, rectangular shape of a typical EDLC cell and shows a maximum capacitance of 31.2 F g^{-1} at a scan rate of 10 mV s^{-1}, which is higher than that of the bare PVDF-based cell (17.3 F g^{-1}) (Table S4, ESI†). GCD curves of each cell at different constant currents (0.25, 0.5, 1, 2, or 4 A g^{-1}) were measured, as shown in Fig. 3(c). The linear voltage–time relationship demonstrates the capacitive behaviour of the cell. The specific capacitance is calculated, showing a capacitance of 38.07 F g^{-1} at 0.5 A g^{-1}. Generally, the EDLC undergoes an ohmic resistance drop or IR drop at the beginning of charge/discharge for an electrolyte potential drop and the contact resistances of the capacitors affect the power performances of the cells. The internal resistance of the EDLC supercapacitor may be improved by using a more conductive current collector. As shown in Fig. 3(d), the cycling stability study of the EDLC supercapacitor was performed using GCD at 1 A g^{-1}. The supercapacitor shows excellent stability over 4000 cycles, retaining $>95\%$ of its original capacitance, while exhibiting $>85\%$ coulombic efficiency. Fig. S8 (ESI†) shows a

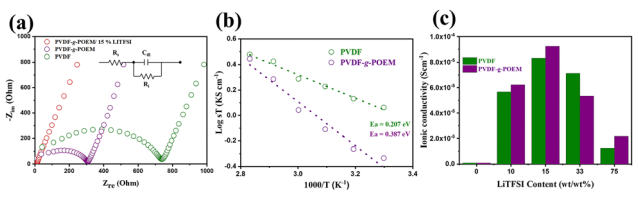

Fig. 2 (a) Nyquist plot of EIS obtained from stainless blocking electrodes for ionic conductivity measurement with an inset showing the simplified RC circuit for solid-state electrolytes. (b) Arrhenius plot of the solid-state electrolytes prepared with 15 wt% LiTFSI content. (c) Bar graphs showing measured ionic conductivity of the solid-state electrolytes prepared from hydrophobic PVDF and amphiphilic PVDF-*g*-POEM double comb copolymer with various LiTFSI contents.

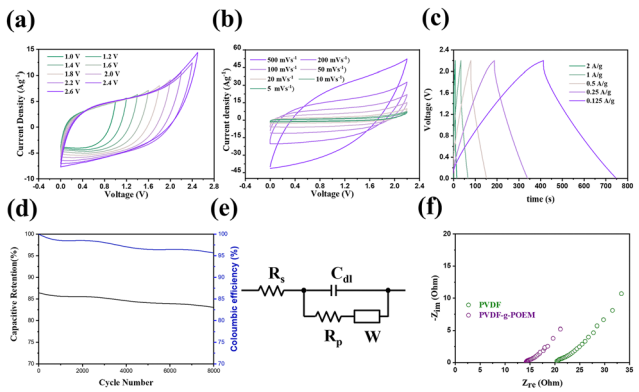

Fig. 3 (a) Cyclic voltammetry of the prepared EDLC cells with different voltage windows and (b) with different scan rates, (c) GCD curves of the EDLC cells, (d) stability test of the prepared cell based on amphiphilic PVDF-*g*-POEM double comb copolymers, (e) graph of the representative equivalent circuit, and (f) Nyquist plot of the EDLC cell based on hydrophobic PVDF and amphiphilic PVDF-*g*-POEM double comb copolymers.

Ragone plot with respect to other EDLC supercapacitor applications. The as-prepared cell displays an energy density of 25.59 kW h kg^{-1} with a power density of 0.275 kW kg^{-1}. Electrochemical impedance spectroscopy was used to evaluate the frequency response behaviour of the EDLC cell and obtain the Nyquist plot of the supercapacitor, as plotted in Fig. 3(e). The inset in Fig. 3(f) illustrates a modified Randles circuit, commonly used to model the impedance behaviour of EDLCs. In this circuit, the resistance (R_p) represents pore or ion migration resistance within the porous structure of the activated carbon electrodes, rather than charge transfer resistance. The model includes the series resistance (R_s), double-layer capacitance (C_{dl}), pore resistance (R_p), and Warburg impedance (W) to capture the ion diffusion behaviour. In the Nyquist plot shown in Fig. 3(e), in the high-frequency region, the EDLC with amphiphilic PVDF-*g*-POEM double comb copolymer exhibits lower series resistance (R_s) compared to PVDF. This indicates enhanced ionic conductivity, while the low-frequency region shows linear behaviour, which indicates the capacitive response of the EDLC.

In summary, this study demonstrates the syntheses of solid-state electrolytes using an amphiphilic PVDF-*g*-POEM double comb copolymer as a matrix. A decrease in crystallinity of the polymer matrix and an increase in ionic pathways due to the polymer nanophase separation resulted in higher observed ionic conductivity of the amphiphilic PVDF-*g*-POEM double comb copolymer based solid-state electrolyte. The EDLC cell showed enhanced performance compared to the cell based on hydrophobic PVDF electrolyte. The EDLC supercapacitors prepared using the amphiphilic PVDF-*g*-POEM double comb copolymer based solid-state electrolyte showed 38.07 F g^{-1} at 0.5 A g^{-1} with an energy density of 25.59 W h kg^{-1} at a power density of 0.275 kW kg^{-1} within the EDLC cell. After 8000 cycles of the cycling study (1 A g^{-1}), the cells displayed a capacitive retention of 95.6%, with an 85% coulombic efficiency. Therefore, the guided synthesis of the amphiphilic PVDF-*g*-POEM double comb copolymer *via* ATRP introduces a novel route for the preparation of solid-state electrolytes, which may result in high-performance energy storage devices, as alternatives to typical PVDF-based electrolytes.

This work was supported by the Technology Innovation Program (20025626) funded by the Ministry of Trade, Industry & Energy (MOTIE, Korea). This research was supported by the Yonsei University Research Fund of 2024-22-0068.

Data availability

The data supporting this article have been included as part of the ESI.†

Conflicts of interest

There are no conflicts to declare.

Notes and references

1 J. Libich, J. Máca, J. Vondrák, O. Čech and M. Sedlaříková, *J. Energy Storage*, 2018, **17**, 224–227.
2 A. Noori, M. F. El-Kady, M. S. Rahmanifar, R. B. Kaner and M. F. Mousavi, *Chem. Soc. Rev.*, 2019, **48**, 1272–1341.
3 P. K. Sharma, A. Arora and S. K. Tripathi, *J. Energy Storage*, 2019, **21**, 801–825.
4 S. Y. Lee, H. J. An, J. Moon, D. H. Kim, K. W. Park and J. T. Park, *Electrochim. Acta*, 2023, **451**, 142291.
5 W. Dong, M. Xie, S. Zhao, Q. Qin and F. Huang, *Mater. Sci. Eng., R*, 2023, **152**, 100713.
6 Q. Dou and H. S. Park, *Energy Environ. Mater.*, 2020, **3**, 286–305.
7 K. Mensah-Darkwa, C. Zequine, P. K. Kahol and R. K. Gupta, *Sustainability*, 2019, **11**, 414.
8 Q. Dou, S. Lei, D.-W. Wang, Q. Zhang, D. Xiao, H. Guo, A. Wang, H. Yang, Y. Li, S. Shi and X. Yan, *Energy Environ. Sci.*, 2018, **11**, 3212–3219.
9 J. X. Lin, Y. Hong, J. Liu, A. Liu, Y. Yao, S. Liu and H. Mi, *New J. Chem.*, 2024, **48**, 8753–8762.
10 T. Guo, D. Zhou, L. Pang, S. Sun, T. Zhou and J. Su, *Small*, 2022, **18**, 2106360.
11 V. T. Nguyen and K.-K. Lee, *ChemSusChem*, 2023, **16**, e202300756.
12 Y. Yu and G. Z. Chen, *Front. Chem.*, 2019, **7**, 272.
13 F. Wan, K. Hu, R. Liu, S. Zhang, S. Li, Y. Lei, D. Yang, C. Wang, Y. Xia and W. Chen, *Chem. Commun.*, 2024, **60**, 7220–7223.
14 P. Lennartz, B. A. Paren, A. Herzog-Arbeitman, X. C. Chen, J. A. Johnson, M. Winter, Y. Shao-Horn and G. Brunklaus, *Joule*, 2023, **7**, 1471–1495.
15 E. Lizundia and D. Kundu, *Adv. Funct. Mater.*, 2021, **31**, 2005646.
16 T. D. Nguyen, S. Roh, M. T. N. Nguyen, Y. Nam, D.-J. Kim, B. Lim, Y. S. Yoon and J. S. Lee, *Chem. Eng. J.*, 2024, **497**, 154430.
17 F. Wan, K. Hu, R. Liu, S. Zhang, S. Li, Y. Lei, D. Yang, C. Wang, Y. Xia and W. Chen, *Chem. Commun.*, 2024, **60**, 7220–7223.
18 X. Qing, J. Li, Z. Wang, M. Chen, J. Lin and X. Lin, *Chem. Commun.*, 2020, **56**, 15533–15536.
19 A. K. Arof, N. E. A. Shuhaimi, S. Amirudin, M. Z. Kufian, H. J. Woo and M. A. Careem, *Polym. Adv. Technol.*, 2014, **25**, 265–272.
20 N. M. Sadiq, R. T. Abdulwahid, S. B. Aziz, H. J. Woo and M. F. Z. Kadir, *Int. J. Biol. Macromol.*, 2024, **265**, 130751.
21 L. S. Cao and M. Yoshio, *Adv. Funct. Mater.*, 2023, **33**, 2300538.
22 J. H. Yoon, W. J. Cho, T. H. Kang, H. Kim, M. Kim and G. Lee, *Macromol. Res.*, 2021, **29**, 509–518.
23 D. E. Apostolides, C. S. Patrickios, T. Sakai, M. Guerre, G. Lopez, B. Améduri, V. Ladmiral, M. Simon, M. Gradzielski, D. Clemens, C. Krumm, J. C. Tiller, B. Ernould and J.-F. Gohy, *Macromolecules*, 2018, **51**, 2476–2488.
24 M. Seidel, S. Jeschke, P. Vettikuzha and H.-D. Wiemhöfer, *Chem. Commun.*, 2015, **51**, 12048–12051.
25 G. H. Choi, S. M. Lim, J. Moon, J. M. Lim, U. C. Baek and J. T. Park, *Chem. Commun.*, 2019, **55**, 11013.
26 R. J. Sengwa and P. Dhatarwal, *Electrochim. Acta*, 2020, **338**, 135890.
27 M. Tripathi, S. M. Bobade and A. Kumar, *Bull. Mater. Sci.*, 2019, **42**, 27.
28 S. Lanceros-Méndez, J. F. Mano, A. M. Costa and V. H. Schmidt, *J. Macromol. Sci. Phys.*, 2001, **40**, 517.
29 S. Toe, F. Chauvet, L. Leveau, J.-C. Remigy and T. Tzedakis, *J. Appl. Electrochem.*, 2023, **53**, 1939–1951.
30 J. Moon, S. Cho, E. Song, K. W. Park, Y. Chae and J. T. Park, *React. Funct. Polym.*, 2021, **169**, 105093.
31 B. Wang, Y. Wu, S. Zhuo, S. Zhu, Y. Chen, C. Jiang and C. Wang, *J. Mater. Chem. A*, 2020, **8**, 5968–5974.

